Jurnal Sains Nuklear Malaysia, 2025, 37(No. 1): 1 – 11
ISSN: 2232-0946

STRUCTURE, MORPHOLOGY AND HYDROGEN STORAGE PROPERTIES OF TI-MN ALLOY SYNTHESIZED BY MECHANICAL ALLOYING TECHNIQUE

Julie Andrianny Murshidi

Materials Technology Group
Industrial Technology Division, Malaysian Nuclear Agency
Bangi, 43000 Kajang, Selangor
Corresponding Author: julie@nm.gov.my

ABSTRACT

Ti-Mn alloy compounds with the composition $TiMn_2$, $Ti_{0.97}Zr_{0.019}Mn_{1.5}Cr_{0.57}$ *and* $Ti_{0.7875}Zr_{0.2625}Mn_{0.8}Cr_{1.2}$ *were synthesised by mechanical alloying technique. An amorphous Ti-Mn alloy was formed when the starting reagents were mechanical alloying for 40 h. The corresponding crystalline phase TiMn was formed when the amorphous alloy was annealed at 800 ℃. The addition of a process control agent (Toluene) leads to the formation of a carbide phase (TiC) in the samples. The presence of impurities, carbide (TiC) and oxide (TiO) phases resulted a decrease in C14 laves phase wt.% in the synthesised samples. Only 37.24, 31.5 and 32.81 wt.% C14 phase were formed in* $TiMn_2$, $Ti_{0.97}Zr_{0.019}Mn_{1.5}Cr_{0.57}$ *and* $Ti_{0.7875}Zr_{0.2625}Mn_{0.8}Cr_{1.2}$ respectively. *The result also showed that the theoretical value of 1.9 hydrogen wt.% could not be reached by these samples.*

Keywords: Mechanical Alloying, Structure, Morphology, Hydrogen Storage

ABSTRAK

Sebatian aloi Ti-Mn dengan komposisi $TiMn_2$, $Ti_{0.97}Zr_{0.019}Mn_{1.5}Cr_{0.57}$ *and* $Ti_{0.7875}Zr_{0.2625}Mn_{0.8}Cr_{1.2}$ *telah disintesis dengan teknik pengaloian secara mekanikal. Aloi Ti-Mn amorfus telah terbentuk apabila reagen permulaan dialoikan secara mekanikal selama 40 jam. Fasa kristal yang sepadan dengan TiMn terbentuk apabila aloi amorfus disepuhlindapkan pada suhu 800 ℃. Penambahan agen kawalan proses (Toluene) membawa kepada pembentukan fasa karbida (TiC) dalam sampel. Kehadiran fasa bendasing, karbida (TiC) dan oksida (TiO) mengakibatkan penurunan fasa laves C14 wt.% dalam sampel yang disintesis. Hanya 37.24, 31.5 dan 32.81 wt.% fasa C14 terbentuk di dalam* $TiMn_2$, $Ti_{0.97}Zr_{0.019}Mn_{1.5}Cr_{0.57}$ *and* $Ti_{0.7875}Zr_{0.2625}Mn_{0.8}Cr_{1.2}$ *masing-masing. Keputusan juga menunjukkan bahawa nilai teori 1.9 hidrogen wt.% tidak dapat dicapai oleh sampel ini.*

Kata kunci: Pengaloian Mekanikal, Struktur, Morfologi, Penstoran Hidrogen

INTRODUCTION

Much research has been undertaken to investigate the hydrogen storage properties of various types of metal hydride families such as Mg-based systems, BCC alloys and intermetallic systems (AB, AB_2 (Laves phase), AB_3 and AB_5) (Nobuko et. al 2017; Nivedhitha et. al 2024; Lototskyy et. al 2015). Intermetallic systems often consist of a stable hydride forming element with an element forming a nonstable hydride.For AB_2, the systems are based on two Laves phases' crystal structures. The crystal structures can be hexagonal, C14 ($MgZn_2$ type) or cubic, C15 ($MgCu_2$ type) (Nobuko et. al 2017; Lototskyy et. al 2015). In these systems the A elements are usually Ti, Zr, Hf, Th or a lanthanide, whilst the B elements can be a variety of transition and non-transition metals.

At the present time AB_2 intermetallic compounds do not satisfy the requirements for mobile storage due to low gravimetric storage capacities (< 2 wt.%) and often high material cost. The storage capacity limitation is less important for stationary storage applications including thermodynamic devices (refrigerator and air conditioner) (Nobuko et. al 2017), fuel cell applications (Charbonnier et. al 2021; Lototskyy et. al 2015) and energy storage units in remote region (Nobuko et. al 2017; Lototskyy et. al 2015). In addition, there are no weight problems in using heavy hydrogen storage tanks if hydrogen is used as a future fuel or fuel additive for sea transportation (because the extra weight can be used to provide ballast to keep the ship stable) (Güther, V. et. Al 1995; Fiori C. et. al, 2015). An inexpensive intermetallic system with the requisite sorption pressure at a desired temperature with adequate kinetics has the potential to be a hydrogen storage material for these markets. The objective of this study was to synthesise and to investigate the properties of TiMn alloys as suitable candidates for material-based hydrogen storage (hydride materials).

EXPERIMENTAL

The starting materials were Ti (Aldrich, 99.7%, -100 mesh), Zr (Aldrich, 99.7%, -100 mesh), Mn (Aldrich, 99.99%) and Cr (Aldrich, 99+%, -325 mesh). Three alloys of nominal composition $TiMn_2$, $Ti_{0.97}Zr_{0.019}Mn_{1.5}Cr_{0.57}$ and $Ti_{0.7875}Zr_{0.2625}Mn_{0.8}Cr_{1.2}$ were prepared by mechanical alloying the starting materials with toluene in a custom-made ball milling canister (650 cm^3 internal volume) attached to a Glen Mills Turbula T2C shaker-mixer. Toluene was used as a process control agent. Milling was performed under a high purity argon atmosphere using a ball-to-powder (mass) ratio of 12:1 with balls of 7.9 mm and 12.7 mm diameter and milling time of 40 h. The as milled samples were removed from the canister in a glove box under argon. The samples were put into the 316 stainless steel sample cell and annealed at 800°C under vacuum for 3h.

The lattice parameter of the alloy before and after hydrogenation was determined by X-Ray Diffraction (XRD) using a Bruker D8 Advance diffractometer (CuKa radiation) with a 2θ range of 30 - 100° using 0.02° steps and a 0.8 s count time per step with operating conditions of 40 kV and 40 mA. Samples were loaded into XRD low background sample holders in an argon glove box and sealed within a poly(methylmethacrylate) (PMMA) air-tight holder to prevent oxygen/moisture contamination during data collection. The structural parameters were refined from the diffraction data using Rietveld refinement in TOPAS (Bruker AXS, Karlsruhe, Germany)

via a fundamental parameters approach. Microstructural observations of as-received and hydrogen cycled alloys were conducted on a Philips XL-30 Scanning Electron Microscopy (SEM) using a secondary electron detector operating at 15 keV. The microscope was coupled with an Oxford Instruments energy dispersive X-Ray spectrometer (EDS) for elemental analysis. Samples were briefly exposed (<1 – 2 min) to air and were not coated with gold prior to imaging in the SEM. The hydrogen sorption properties of the alloy were determined using a custom-built automated Sieverts apparatus (details can be found elsewhere (Marangio, F. et. Al 2011). Before any pressure-composition isotherm (PCI) measurements were undertaken the sample was first evacuated for 1 h at 25 °C to remove any adsorbed gas. Activation of the alloy was then undertaken by first introducing 90 – 96 bars of hydrogen into the sample chamber at room temperature for 1 h, followed by an evacuation step. This hydrogen absorption/ desorption activation cycle was undertaken 3 times. After completion of the activation process, the residual hydrogen within the sample was removed via evacuation at room temperature for 24 h.

RESULTS AND DISCUSSION

Fig. 1 (left) shows that after 12 h of milling, both Ti and Mn peaks were still present. The diffraction peaks are slightly broader compare to those after milling for 2 h. TiC peaks were observed in the XRD pattern due to addition of toluene during milling process. TiC and TiO phases have similar major XRD peaks, so those denoted in Fig. 1 (left) most likely represent the presence of a combination of both TiC and TiO in the sample. After 40 h milling, the sample became quite nanocrystalline. All peaks except the strongest peak of Mn become nearly invisible. The position of the remaining peak of Mn was shifted to a lower angle. The as-milled $TiMn_2$ sample was then annealed at 800°C under vacuum for 3 hours. The XRD pattern shown in Fig. 1 (right) consists of peaks related to $TiMn_2$, TiC, TiO and Mn. The $TiMn_2$ phase was easily indexed on the basis of the hexagonal C14-Laves phases (*$P6_3$ / mmc* space group). The calculated lattice parameters determined by Rietveld analysis are listed in Table 1. This result showed that the crystalline phase of Ti-Mn could be achieved through annealing of its milled powder. This is consistent with previous study of synthesising crystalline $Ti_{50}Mn_{50}$ alloy by milling for 40 h and annealing at 700 - 900°C (Chen, C. C. et. al 1993). Annealing was also reported to increase the homogeneity of the crystal structure of the sample (Gamo, T. et. al 1995).

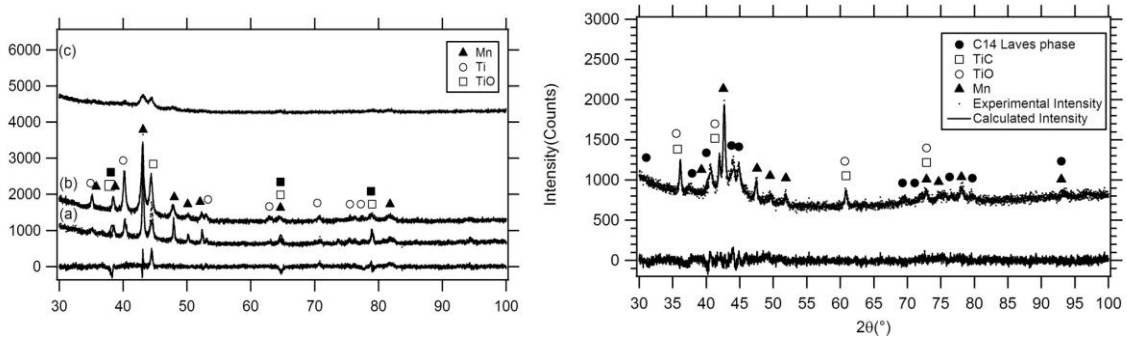

Figure 1: XRD pattern of as-milled $TiMn_2$ powders using BPR of 12:1 at (a) 2 h, (b) 12 h and (c) 40 h milling times (left) and annealed $TiMn_2$ at 800°C (right).

During mechanical alloying, powder particles are subjected to high-energy collision, which causes the powder particles to be cold-welded together and fractured. The essential condition for a successful mechanical alloying process is the balance between cold-welding and fracturing. However, this balance may not be obtained by the milling process itself, especially when soft materials are used. For such cases, cold welding among powder particles and between powder particles and milling tools becomes a serious problem. In order to obtain the balance between the welding and fracturing, a PCA is added in the milling process. The PCA adsorbs on the surface of the powder particles and minimizes the cold-welding effect (Suryanarayana, C. 2001). It is known that Mn is much softer and is more easily to be cold welded to the milling tools compare to Ti. Brinell hardness reported for Ti and Mn are 716 MNm^{-2} and 196 MNm^{-2} respectively. To avoid this, toluene was used as a PCA. However, the addition of toluene resulted in the formation of TiC in the sample. Hydrocarbon PCAs have been reported to introduce carbon and/or oxygen into the powder particles, resulting in the formation of carbides and oxides which are uniformly dispersed in the matrix.

Table 1: Rietveld analysis for phase composition and lattice parameter calculated from XRD patterns in Fig. 1 and 4). Mathematical fitting uncertainties are provided (2 standard deviations).

Alloys	Annealed (wt.%)		Lattice parameters		
			a(nm)	c(nm)	V(nm^3)
$TiMn_2$ (BPR 12:1)	C14 TiO/TiC Mn	37.24±0.5 22.16±0.5 40.59±0.5	0.4821	0.7856	0.1581
$Ti_{0.97}Zr_{0.019}Mn_{1.5}Cr_{0.57}$	C14 TiO/TiC Mn	31.5±1.2 10.31±0.8 58.19±1.6	0.4837	0.7892	0.1600
$Ti_{0.7875}Zr_{0.2625}Mn_{0.8}Cr_{1.2}$	C14 TiO/TiC Cr Zr	32.81±0.5 16.41±0.7 39.98±0.5 10.79±0.5	0.4859	0.7940	0.1623
$TiMn_2$ C14 Laves phase PDF No. 07-0133	-	-	0.4825	0.7917	0.1596

An XRD pattern of the starting Ti powder (Fig. 2) also revealed that a minor oxide phase already presents in the purchased product. Ti powder is known to be more reactive with oxygen when in extremely small particle size (in this case -100 mesh powder) (Suryanarayana, C. 2001). The strongest peak in the starting Ti powder at 36.6° could not be indexed to any known pure Ti element or oxide and is an unknown component. This indicates that there could be an impurity in the Ti starting powder. As a result of these impurity, carbide and oxide phases, the level of Ti available to form $TiMn_2$ alloy was reduced and a high level of Mn was left in the sample. Based on Rietveld analysis in Table 1, only 37.24 wt.% $TiMn_2$ phase was formed in the sample.

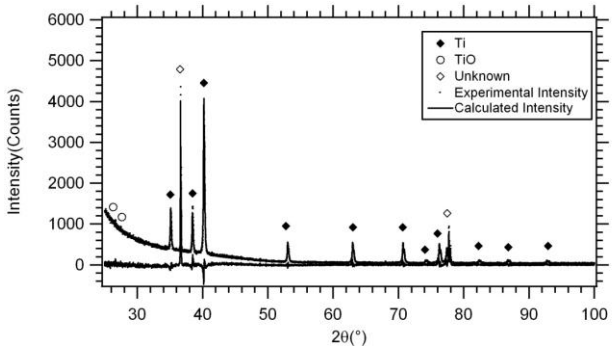

Figure 2:.XRD pattern of starting powder Ti.

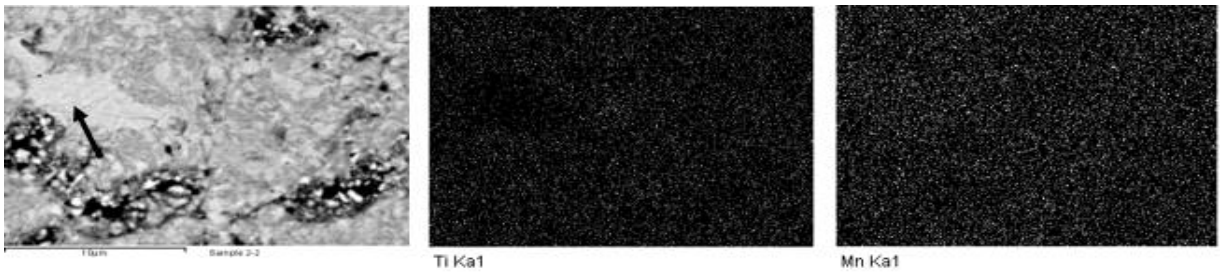

Figure 3: BF image and the corresponding EDS elemental mapping of $TiMn_2$ (bright region is shown by the black arrow)

Fig. 3 of BF image shows no sign of a lamellae structure. At the beginning of mechanical alloying, different elemental powder particles are partially mixed and large blocks containing coarse layers have formed (Mahboubi, S. et. al 2017). Formation of a coarse lamellae structure of initial powders may be due to low plastic deformation. Continuous cold welding and fracturing result coarse layers to be fractured and flattened and subsequently fresh metal surfaces welded together. This results in formation of fine layered structure and inter-diffusion of elements across layers. With further milling up to 40 h, the layers became hardly detectable. The elemental mapping of the sample shows the characteristic energies of Ti and Mn. Both elements are distributed homogeneously throughout the sample except the bright region. The brighter region contains more Mn and less Ti than the darker region. This observation indicates that there may not be enough Ti content to diffuse in the (Ti, Mn) matrix forming different contrast in the sample.

Fig. 4 show the XRD patterns of $Ti_{0.97}Zr_{0.019}Mn_{1.5}Cr_{0.57}$ and $Ti_{0.7875}Zr_{0.2625}Mn_{0.8}Cr_{1.2}$ samples respectively prepared by mechanical alloying the starting reagents using a BPR of 12:1 for 40 hours. 3 drops of toluene were added to the starting reagents during milling. Then the as-milled samples were annealed at 800°C under vacuum for 3 hours. Both XRD patterns consist of peaks related to $TiMn_2$, TiC, TiO and Mn. As a result of impurity, carbide and oxide phases' presence in these samples, the level of Ti available to form $TiMn_2$ alloy were reduced. Based on Rietveld analysis in Table 1, only 31.5 wt.% and 32.81 wt.% $TiMn_2$ phase was formed in $Ti_{0.97}Zr_{0.019}Mn_{1.5}Cr_{0.57}$ and $Ti_{0.7875}Zr_{0.2625}Mn_{0.8}Cr_{1.2}$ respectively. For $Ti_{0.7875}Zr_{0.2625}Mn_{0.8}Cr_{1.2}$, due to its low wt.% $TiMn_2$ phase formed and the high level of substitute elements used (Zr and Cr),

only limited levels of partially substitution could take place in the sample. As a result, peaks related to Cr and Zr phases were still detected in this sample as shown in Fig. 4. The effects of partial substitution of Zr for Ti and Cr for Mn are shown in Table 1. With increasing Zr and Cr content, the lattice parameter of the C14- Laves phases were also increased. This is due to the atom radius of Zr and Cr are bigger than that of Mn.

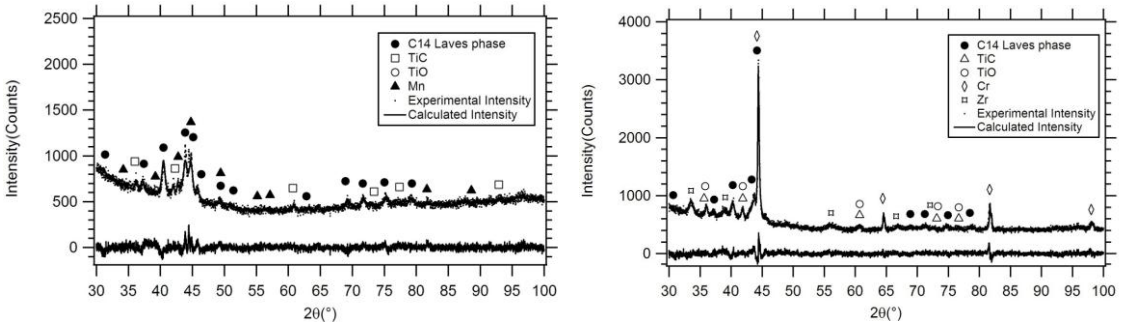

Figure 4: XRD pattern of $Ti_{0.97}Zr_{0.019}Mn_{1.5}Cr_{0.57}$ (left) and $Ti_{0.7875}Zr_{0.2625}Mn_{0.8}Cr_{1.2}$ (right).

Fig. 5 shows the BF image of the sample$Ti_{0.97}Zr_{0.019}Mn_{1.5}Cr_{0.57}$ and its corresponding EDS elemental mapping. All elements are distributed homogeneously throughout the sample except the bright region. The brighter region contains more Cr, Mn and less Ti than the darker region. This indicates that the alloy was composed of the C14 Laves phase (dark region) and some impurity phase of Mn and Cr (bright region). This result is also similar with sample $Ti_{0.7875}Zr_{0.2625}Mn_{0.8}Cr_{1.2}$ as shown in Fig. 6. However, Zr element was also detected in this sample due to high level of Zr in sample $Ti_{0.7875}Zr_{0.2625}Mn_{0.8}Cr_{1.2}$ compare to $Ti_{0.97}Zr_{0.019}Mn_{1.5}Cr_{0.57}$.

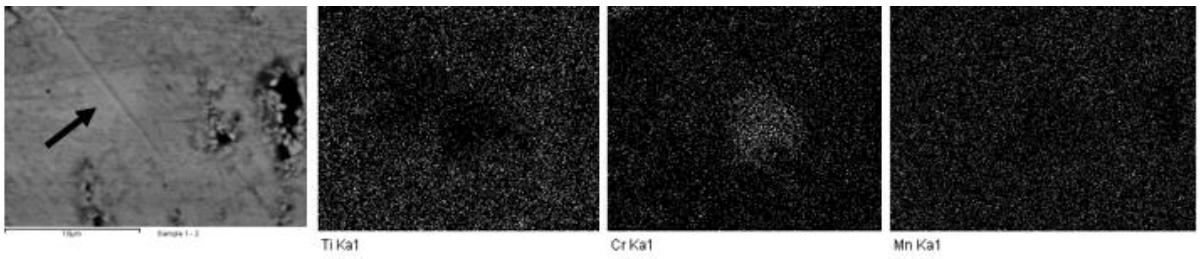

Figure 5: BF image and the corresponding EDS elemental mapping of $Ti_{0.97}Zr_{0.019}Mn_{1.5}Cr_{0.57}$ (bright region is shown by the black arrow)

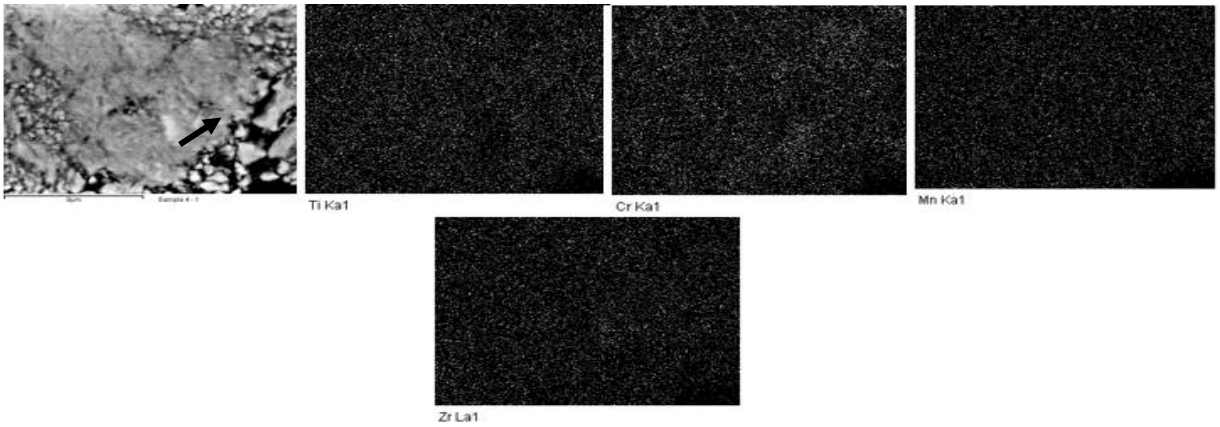

Figure 6: BF image and the corresponding EDS elemental mapping of $Ti_{0.7875}Zr_{0.2625}Mn_{0.8}Cr_{1.2}$ (bright region is shown by the black arrow).

EDS data verifies the presence of high quantities of Ti and Mn in all samples (Fig. 7a, b and c). EDS also showed the existence of Fe, Cr and Ni for all samples, as a result of an excessive wear of the milling tools. Zr and Cr are the results of partial substitution of Ti and Mn in sample $Ti_{0.97}Zr_{0.019}Mn_{1.5}Cr_{0.57}$ (Fig. 7b) and $Ti_{0.7875}Zr_{0.2625}Mn_{0.8}Cr_{1.2}$ (Fig. 7c). Cr contents are higher in Fig. 7c due to high level of Cr in sample $Ti_{0.7875}Zr_{0.2625}Mn_{0.8}Cr_{1.2}$ compare to sample $Ti_{0.97}Zr_{0.019}Mn_{1.5}Cr_{0.57}$. C comes from using toluene as a PCA.

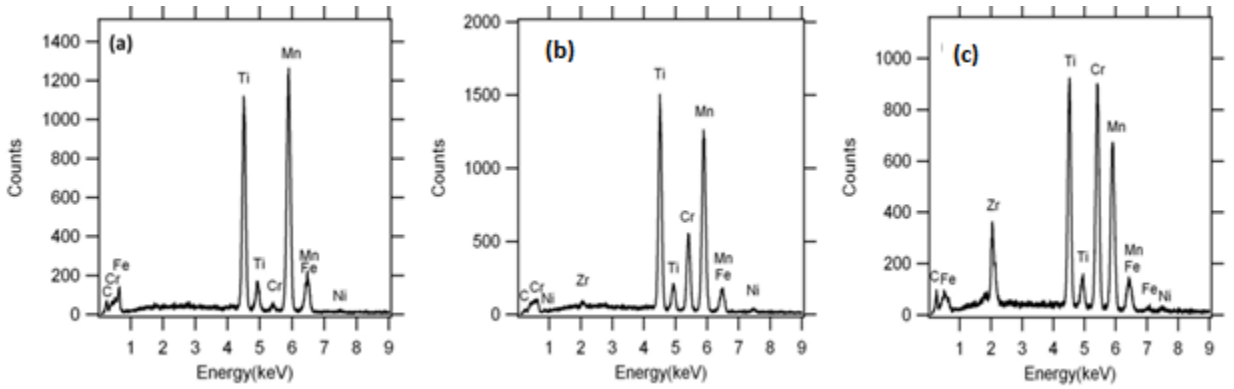

Figure 7: EDS spectra of (a) $TiMn_2$, (b) $Ti_{0.97}Zr_{0.019}Mn_{1.5}Cr_{0.57}$ and (c) $Ti_{0.7875}Zr_{0.2625}Mn_{0.8}Cr_{1.2}$.

Table 2 show the maximum hydrogen wt.% of sample $TiMn_2$, $Ti_{0.97}Zr_{0.019}Mn_{1.5}Cr_{0.57}$ and $Ti_{0.7875}Zr_{0.2625}Mn_{0.8}Cr_{1.2}$ respectively. Maximum hydrogen absorbed in $TiMn_2$, $Ti_{0.7875}Zr_{0.2625}Mn_{0.8}Cr_{1.2}$and $Ti_{0.97}Zr_{0.019}Mn_{1.5}Cr_{0.57}$ sample were only 0.15 wt.%, 0.19 wt.% and 0.34 wt.% respectively due to impurities phases. It was clear that theoretical value of 1.9 hydrogen wt.% would not be reached by these samples. High energy milling and longer milling time lead to heavy deformation of samples and high oxidisation of sample (Suryanarayana, C. 2001). It is believed that these crystal deformities and together with impurity phases (oxides, carbides, MnCrZr) both contribute to the low hydrogen weight capacity achieved in these samples.

Table 2: Hydrogen contents in $TiMn_2$, $Ti_{0.97}Zr_{0.019}Mn_{1.5}Cr_{0.57}$ and $Ti_{0.7875}Zr_{0.2625}Mn_{0.8}Cr_{1.2}$ samples.

Cycle	Hydrogen Absorption in $TiMn_2$	Maximum hydrogen wt.%
1	Initial pressure of 96.30 bar was applied at RT for 1 h and the final pressure was 47.98 bar.	0.15
2	Initial pressure of 94.35 bar was applied at RT for 1 h and the final pressure was 47.10 bar.	0.15
3	Initial pressure of 94.68 bar was applied at RT for 1 h and the final pressure was 47.18 bar.	0.12
Cycle	Hydrogen contents in $Ti_{0.97}Zr_{0.019}Mn_{1.5}Cr_{0.57}$	Maximum hydrogen wt.%
1	Initial pressure of 96.19 bar was applied at RT for 1 h and the final pressure was 49.29 bar.	0.19
2	Initial pressure of 96.74 bar was applied at RT for 1 h and the final pressure was 49.53 bar.	0.17
3	Initial pressure of 96.88 bar was applied at RT for 1 h and the final pressure was 49.52 bar.	0.18
Cycle	Hydrogen contents in $Ti_{0.7875}Zr_{0.2625}Mn_{0.8}Cr_{1.2}$	Maximum hydrogen wt.%
1	Initial pressure of 90.81 bar was applied at RT for 1 h and the final pressure was 42.25 bar.	0.32
2	Initial pressure of 90.65 bar was applied at RT for 1 h and the final pressure was 42.29 bar.	0.34
3	Initial pressure of 90.54 bar was applied at RT for 1 h and the final pressure was 42.12 bar.	0.28

From the hydrogen absorption measurement, the kinetics of the samples (Fig. 8) was determined. The kinetics of hydrogen absorption was measured by recording wt.% data at room temperature. It was found that the sample had very fast kinetics, with alloys reaching hydrogen absorption equilibrium within 30 minutes.

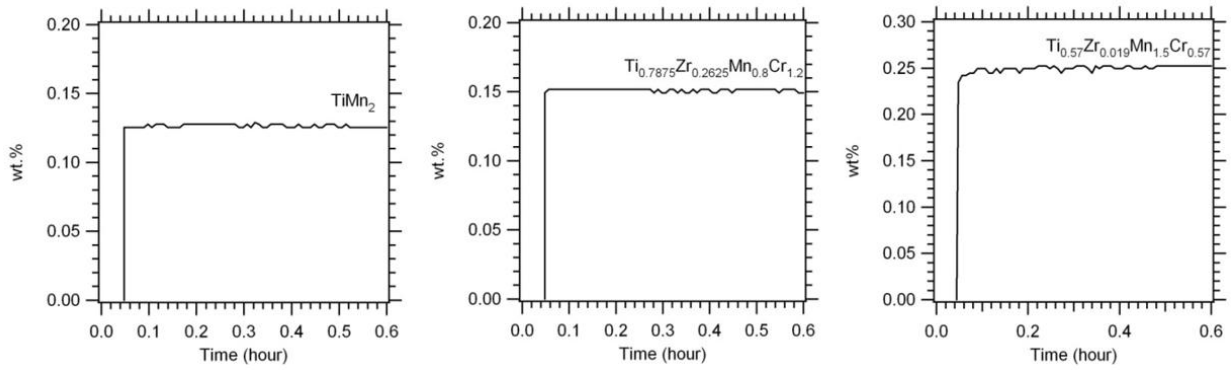

Figure 8: Hydrogenation kinetics on absorption at room temperature for $TiMn_2$, $Ti_{0.7875}Zr_{0.2625}Mn_{0.8}Cr_{1.2}$ and $Ti_{0.97}Zr_{0.019}Mn_{1.5}Cr_{0.57}$ samples after three activation cycles.

CONCLUSION

Ti-Mn alloy compounds with the composition $TiMn_2$, $Ti_{0.97}Zr_{0.019}Mn_{1.5}Cr_{0.57}$ and$Ti_{0.7875}Zr_{0.2625}Mn_{0.8}Cr_{1.2}$ have been synthesised. A nanocrystalline Ti-Mn alloy was formed when the starting reagents were mechanical alloying for 40 h, using a ball-to-powder (mass) ratio of 12:1 and annealed at 800°C. The addition of PCA leads to the formation of carbide phase (TiC) in the samples. The presence of impurity, carbide (TiC) and oxide (TiO) phases resulted a decrease in C14 laves phase wt.% in the synthesised samples. Only 37.24, 31.5 and 32.81 wt.% C14 phase were formed in $TiMn_2$, $Ti_{0.97}Zr_{0.019}Mn_{1.5}Cr_{0.57}$ and $Ti_{0.7875}Zr_{0.2625}Mn_{0.8}Cr_{1.2}$ respectively. The result also showed that the theoretical value of 1.9 hydrogen wt.% could not be reached by these samples. Therefore, for future work, samples with an oxygen scavenger and an effective PCA that will not react with the starting reagents should be studied.

ACKNOWLEDGEMENTS

The author would like to thank the Government of Malaysia for funding and all personnel involved for their direct or indirect support to carry out this project.

REFERENCES

Charbonnier V. , Enoki H. , Asano K. , Kim H. , Sakaki K., (2021), Tuning the hydrogenation properties of $Ti_{1+y}Cr_{2-x}Mn_x$ laves phase compounds for high pressure metal-hydride compressors, *International Journal of Hydrogen* Energy, 46: 36369-36380

Chen, C. C., Chin, Z. H., Perng, T. P., (1993), Preparation and crystallization of $Ti_{50}Mn_{50}$ amorphous alloy, *Materials Science and Engineering: A*, *173*: 381 - 384.

Cingi, M. M., O. Guleryuz, H. Baydogan, M. Cimenoglu, H. Kayali, E.S. (2007), High Cyclic Fatigue Bahaviour of Thermally Oxidized Ti6Al4V Alloy, *Materials Science Forum*, *561/565*: 2179 - 2182.

El-Eskandarany, M.S., (2001), *Mechanical Alloying for Fabrication of Advanced Engineering Materials*, William Andrew Publishing, New York. 142 – 173.

Fiori C., Dell'Era A., Zuccari F., Santiangeli A., D'Orazio A., Orecchini F., (2015), Hydrides for submarine applications: Overview and identification of optimal alloys for air independent propulsion maximization, International Journal of Hydrogen Energy, 40: 11879-11889.

Gamo, T., Moriwaki, Y., Yanagihara, N., Yamashita, T., Iwaki, T., (1985), Formation and properties of titanium-manganese alloy hydrides, *International Journal of Hydrogen Energy*, *10*:39 - 47.

Güther, V.; Otto, A., (1999), Recent developments in hydrogen storage applications based on metal hydrides, *Journal of Alloys and Compounds*, 293 - 295: 889 - 892.

Lototskyy M. , Satya Sekhar B., Muthukumar P., Linkov V., Pollet B. G., (2015), Niche applications of metal hydrides and related thermal management issues, *Journal of Alloys and Compounds*, 645: S117-S122.

Lototskyy, M. V., Tolj, I., Pickering, L., Sita, C., Barbir, F., & Yartys, V. (2017). The use of metal hydrides in fuel cell applications. *Progress in Natural Science: Materials International*, 27(1), 3–20.

Mahboubi, S. A., Karimzadeh F., Enayati M., (2012), Formation mechanism and characterization of nanostructured Ti6Al4V alloy prepared by mechanical alloying, *Materials & Design*, 37: 152-160,

Marangio, F., Pagani, M., Santarelli, M., Calì, M., (2011), Concept of a high pressure PEM electrolyser prototype *International Journal of Hydrogen Energy,* 36: 7807 - 7815.

Mohd N. I., Teuku H., Jonathan G., Abu B., (2022), High-pressure PEM water electrolyser: A review on challenges and mitigation strategies towards green and low-cost hydrogen production, *Energy Conversion and Management* 268(486):115985

Nivedhitha K.S, Beena T., Banapurmath N.R., Umarfarooq M.A., Venkatesh R., Manzoore E. M. S, (2024), Advances in hydrogen storage with metal hydrides: Mechanisms, materials, and challenges, *International Journal of Hydrogen Energy*, 61: 1259-1273.

Nobuko H., Hirotaka A., Tessui Nakagawa., Hiroki Higa., Masayoshi I., Daichi H., Tomohiro T., Itoko S., Kohta A., Yumiko N., Akitoshi F., Shinichi M., (2017), Effect of CO_2 on hydrogen absorption in Ti-Zr-Mn-Cr based AB_2 type alloys, *Journal of Alloys and Compounds*, 705: 507-516

Suryanarayana, C. (2001), Mechanical alloying and milling, *Progress in Materials Science*, 46: 1 - 184.

Villeroy, B., Cuevas, F., Bettembourg, J., Olier, P., Latroche, M., (2006), Influence of the Ti/Zr ratio and the synthesis route on hydrogen absorbing properties of (Ti1−xZrx)Mn1.5V0.5 alloys, *Journal of Physics and Chemistry of Solids*, 67(5-6): 1281–1285.